Electronic Supplementary Material (ESI) for CrystEngComm.

Supplementary information for: "Naphthalene crystal shape prediction from molecular dynamics simulations"

Zoran Bjelobrk,[†] Pablo M. Piaggi,[‡,¶] Thilo Weber,[†] Tarak Karmakar,[§,¶]

Marco Mazzotti,[*,†] and Michele Parrinello[*,§,¶]

[†]*Institute of Process Engineering, ETH Zürich, CH-8092, Switzerland*

[‡]*Theory and Simulation of Materials (THEOS), École Polytechnique Fédérale de Lausanne, CH-1015 Lausanne, Switzerland*

[¶]*Facoltà di Informatica, Istituto di Scienze Computationali, Università della Svizzera italiana, via Giuseppe Buffi 13, CH-6900 Lugano, Switzerland*

[§]*Department of Chemistry and Applied Biosciences, ETH Zürich, c/o USI Campus, via Giuseppe Buffi 13, CH-6900 Lugano, Switzerland*

E-mail: marco.mazzotti@ipe.ethz.ch; parrinello@phys.chem.ethz.ch

Parameters used for biased simulations

Parameters of the surface layer crystallinity CV, s_{slc}, and biased CV, s, used in the simulations are summarized in Table 1. The well-tempered Metadynamics parameters are summarized in Table 2, where Δs is the bin size of the grid on which the positions of the Gaussian potentials are discretized.

Table 1: Surface layer crystallinity CV parameters used for the biased simulations.

	$\{00\bar{1}\}$	$\{1\bar{1}0\}$	$\{20\bar{1}\}$
θ_1 [rad]	0.0000	0.0000	0.0000
θ_2 [rad]	0.4400	0.4400	0.4400
θ_3 [rad]	2.7016	2.7016	2.7016
θ_4 [rad]	3.1416	3.1416	3.1416
σ_1 [rad]	0.15	0.15	0.15
σ_2 [rad]	0.15	0.15	0.15
σ_3 [rad]	0.15	0.15	0.15
σ_4 [rad]	0.15	0.15	0.15
n_{cut} [-]	4	4	4
r_{cut} [nm]	0.65	0.90	0.90
a [-]	15	15	15
ζ_c [-]	0.5884	0.5958	0.5958
ζ_l [-]	0.6304	0.6229	0.6229
σ_c [-]	2000	2000	2000
σ_l [-]	2000	2000	2000
χ [-]	0.7	0.5	0.5

Table 2: Well-tempered Metadynamics parameters used for the biased simulations.

	$\{00\bar{1}\}$	$\{1\bar{1}0\}$	$\{20\bar{1}\}$
W [kJ/mol]	0.8	0.5	0.5
σ_W [-]	0.7	0.4	0.4
γ [K]	12	10	8
τ [ps]	1	1	1
Δs [-]	0.14	0.08	0.08

Table 3: GAFF parameters for naphthalene.

atom name	GAFF atom type	RESP charge [e]	mass [g/mol]	x [nm]	y [nm]	z [nm]
C1	ca	-0.116476	12.010	0.000	0.244	-0.071
C2	ca	-0.116476	12.010	0.000	0.244	0.071
C3	ca	-0.264483	12.010	0.000	0.125	0.140
C4	ca	-0.264483	12.010	0.000	-0.125	0.140
C5	ca	-0.116476	12.010	0.000	-0.244	0.071
C6	ca	-0.264483	12.010	0.000	0.125	-0.140
C7	ca	-0.116476	12.010	0.000	-0.244	-0.071
C8	ca	0.216029	12.010	0.000	0.000	0.072
C9	ca	0.216029	12.010	0.000	0.000	-0.072
C10	ca	-0.264483	12.010	0.000	-0.125	-0.140
H1	ha	0.127069	1.008	0.000	0.338	-0.125
H2	ha	0.127069	1.008	0.000	0.338	0.125
H3	ha	0.145875	1.008	0.000	0.124	-0.249
H4	ha	0.145875	1.008	0.000	0.124	0.249
H5	ha	0.145875	1.008	0.000	-0.124	0.249
H6	ha	0.127069	1.008	0.000	-0.338	0.125
H7	ha	0.127069	1.008	0.000	-0.338	-0.125
H8	ha	0.145875	1.008	0.000	-0.124	-0.249

Naphthalene force field

The general AMBER force field (GAFF)[1] parameters of naphthalene obtained by the procedure described in the main text are listed in Table 3 (check Figure 1 for the numbering of the atoms).

To estimate how well the naphthalene GAFF reproduces the experimental crystal structure, simulations of a $\sim 3 \times 3 \times 3$ nm^3 crystal were performed under NPT conditions with anisotropic pressure coupling[2] at 1 bar and 300 K. Figure 2 shows the radial distribution function, $g(r)$, and the PDFs of the vector angles, $p(\theta_{1257})$ and $p(\theta_{89})$. The red lines were computed from XRD measurement data[3] and the three blue lines are simulation results at times 3 ns, 6 ns, and 9 ns. The center of mass of carbon atoms 8 and 9 were defined as molecule center and the vector angle definitions are shown in Figure 1. Simulation results for $g(r)$, $p(\theta_{1257})$, and $p(\theta_{89})$ show all satisfactory agreement with the XRD data.

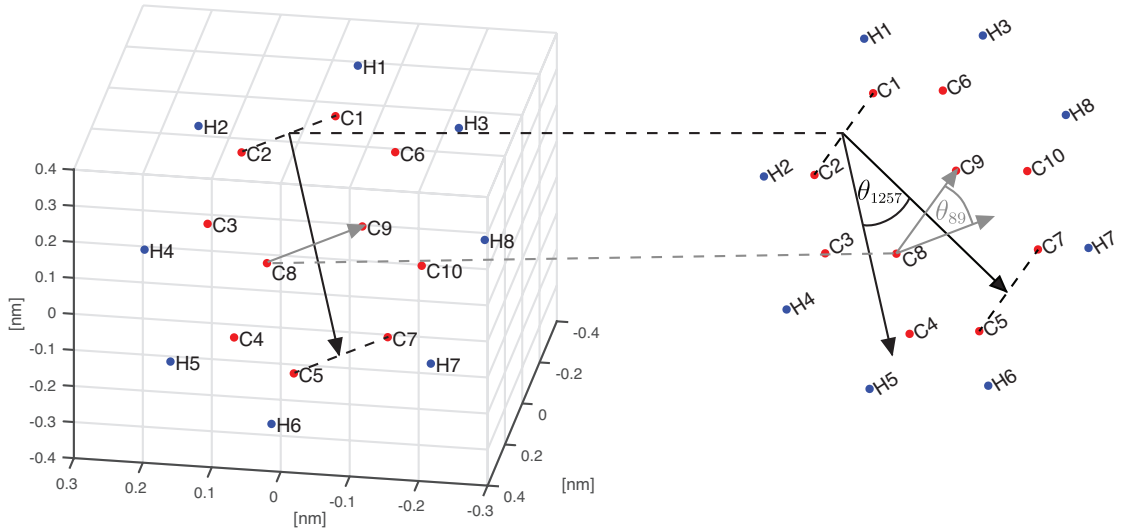

Figure 1: Naphthalene atom numbering and vector angle definitions of θ_{1257} and θ_{89}.

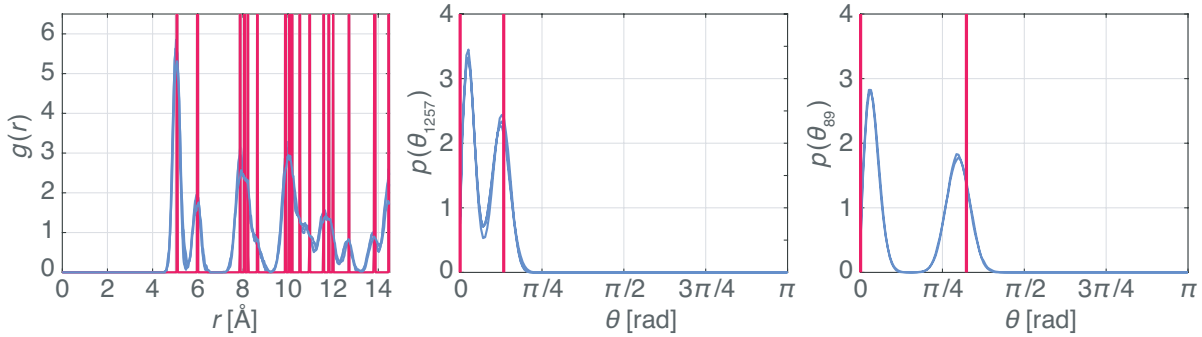

Figure 2: Histograms of the radial distribution function $g(r)$, left, and the vector angle porbability density functions $p(\theta_{1257})$, center, and $p(\theta_{89})$, right. Histograms of the simulation (in blue) are shown at simulation times 3 ns, 6 ns, and 9 ns, and are in good agreement with the histograms obtained from the XRD measurements at 300 K (in red).

The melting temperature of the naphthalene GAFF was estimated by simulation runs of a roughly 3×3×3 nm^3 crystal slab exposing the $\{1\bar{1}0\}$ face to a liquid naphthalene phase around twice the size of the crystal. Simulations were performed at different temperatures under NPT conditions with the velocity rescale thermostat[4] and semi-isotropic Parrinello-Rahman barostat[2] (L_x and L_y coupled, L_z decoupled) at 1 bar. Growth of the crystal slab was observed at temperatures below 330 K, while at temperatures at and above 330 K the crystal slab was melting. The trajectories of the system crystallinity, s_c, for the different temperatures are presented in Figure 3. The CV s_c takes all solute molecules of the system into account and is reported in Reference 5. The simulated melting temperature of $\sim$ 330 K lies sufficiently close to the experimental one at 352 - 354 K.[6]

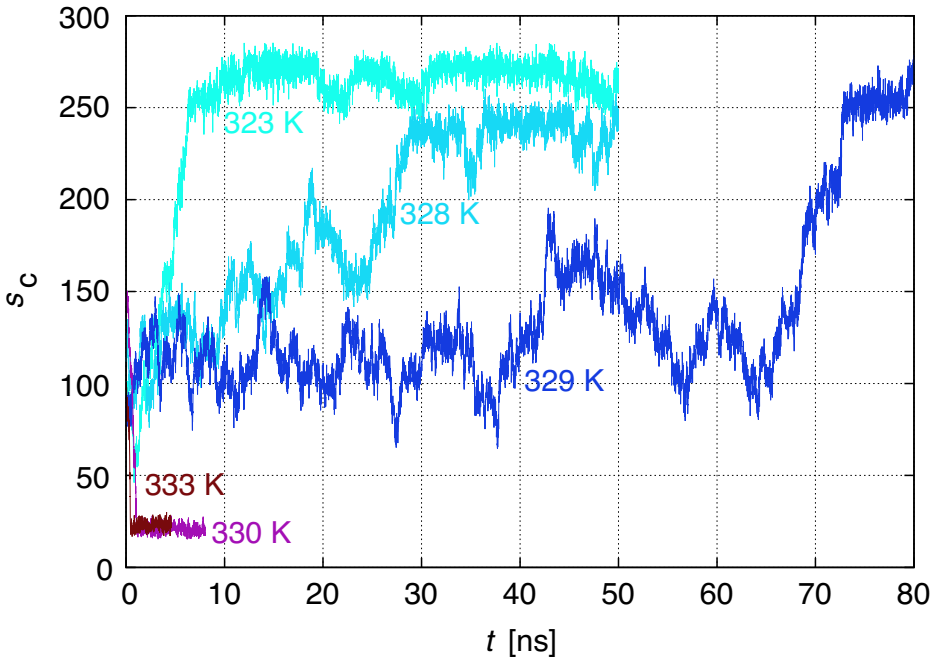

Figure 3: System crystallinity CV, s_c, in dependence of time for different temperatures. The seed crystal is associated with a s_c value of $\sim$ 100; For temperatures below 330 K, the crystalline phase grows until the liquid phase is completely converted into the crystalline state (at $s_c \approx 270$). At temperatures at and above 330 K, the crystal dissolves very quickly until only the liquid phase remains (at $s_c \approx 20$).

To obtain the initial configurations for both the crystallographic structure comparison and for the melting temperature, the equilibration procedure was used which is described in

the following section. All MD simulation parameters which were utilized for the simulations above and are not explicitly mentioned, are described in the main text.

Simulation setup equilibration

All equilibration steps were performed with Gromacs 2016.5[7] using the velocity rescaling thermostat,[4] periodic boundary conditions, the particle mesh Ewald approach[8] for the electrostatic interactions, and the LINCS algorithm[9,10] to constrain the covalent bonds involving hydrogens. The non-bonded cutoff was set to 1 nm.

For each crystal face, the following procedure was performed to obtain initial configurations for the three slowest growing naphthalene crystal faces, $\{00\bar{1}\}$, $\{1\bar{1}0\}$, and $\{20\bar{1}\}$.[11] A seed crystal was constructed from the XRD data[3] with the face of interest perpendicular to the z-axis. The crystal system was first minimized with the conjugate gradient algorithm with a tolerance on the maximum force of 50 kJ mol^{-1} nm^{-1}, and subsequently equilibrated under NVT conditions for 1 ns, at 280 K and an integration time step of 0.5 fs. A temperature of 280 K was chosen to match the temperature of the experiments reported by Lovette *et al.*[12]

In a second step, the system was equilibrated for 10 ns under NPT conditions with the anisotropic Parrinello-Rahman barostat[2] at 1 bar, 280 K, and with the same integration time step of 0.5 fs. From the NPT equilibration (while not considering the first 1 ns), the frame with box size values L_x, L_y, and the ratio L_x/L_y, closest to the average values, was considered. The averaged crystal configuration was then submerged in the solution by extending the box length L_z to more than four times the crystal length in the z-direction and filling the box with naphthalene and ethanol molecules using the genbox utility of Gromacs.[10]

For the system containing the crystal as well as the solution, the same minimization and equilibration steps were performed. For the NPT equilibration, the box expansion was only allowed in the z-direction, keeping L_x and L_y constant. The simulation frame with

box length L_z closest to the average one (again omitting the first 1 ns) was picked as initial configuration for the last equilibration step involving the CμMD algorithm.[13]

To obtain the final initial configuration which holds the targeted concentrations in both control regions, the system had to undergo an equilibration procedure, in which the average concentration profile along the z-axis becomes static. A simulation of 25 ns ensured to reach an adequate convergence. The last frame of the concentration profile equilibration for each face and supersaturation was used for the simulations. The numerical parameter values of the CμMD algorithm are shown in Table 4.

The number of molecules and simulation box lengths used for the biased simulations are presented in Table 5.

Table 4: Parameters used for the CμMD algorithm.

k [kJ/mol]	1500
ω [-]	0.04
z_{TR} [-]	0.11
z_{CR} [-]	0.26
z_{F} [-]	0.33
Δz [-]	1/120

Table 5: Number of molecules and simulation box lengths used for the biased simulations.

face	number of molecules [-]		box lengths [nm]		
	naphthalene	ethanol	L_x	L_y	L_z
$\{20\bar{1}\}$	380	1053	2.975	3.577	16.560
$\{1\bar{1}0\}$	360	951	3.035	3.172	16.936
$\{00\bar{1}\}$	360	951	3.287	2.985	16.655

CμMD concentration profiles

Parameters used in the CμMD algorithm are shown in Table 4. And the corresponding concentration profiles for all six biased simulation runs (each performed for 1 μs) are shown in Figure 4. The crystal surface was biased on the right side of the crystal shown in the middle

of each graph, while the surface on the left was not biased at all. The target concentrations in both control regions were met with satisfactory accuracy.

Solubility estimation

To our knowledge, no simple algorithm exists for computing the exact solubility of naphthalene in ethanol at the given concentrations. However it is possible to estimate the limits within the solubility is located by the use of the CμMD algorithm and long enough simulation runs. Figure 5 shows the system crystallinity CV, s_c, trajectories for different runs of the three simulation series, each under different concentrations, $C = 0.6$ nm^{-3}, $C = 0.8$ nm^{-3}, and $C = 1.0$ nm^{-3}. For each concentration series the total time of all simulation runs sums up to 7.5 μs. In case of $C = 0.6$ nm^{-3}, six dissolution events while no growth events were observed. For $C = 0.8$ nm^{-3} two dissolution and two growth events were observed. While for $C = 1.0$ nm^{-3}, no dissolution, however five growth events were observed. The solubility is therefore estimated to reside around $C = 0.8$ nm^{-3}.

Constraint of seed crystal movement

For the biased simulations, the center of mass of the two most inner layers of each seed crystal was constrained in its movement along the z axis with a harmonic potential. The force constant was set to 1500 kJ/mol for all three faces.

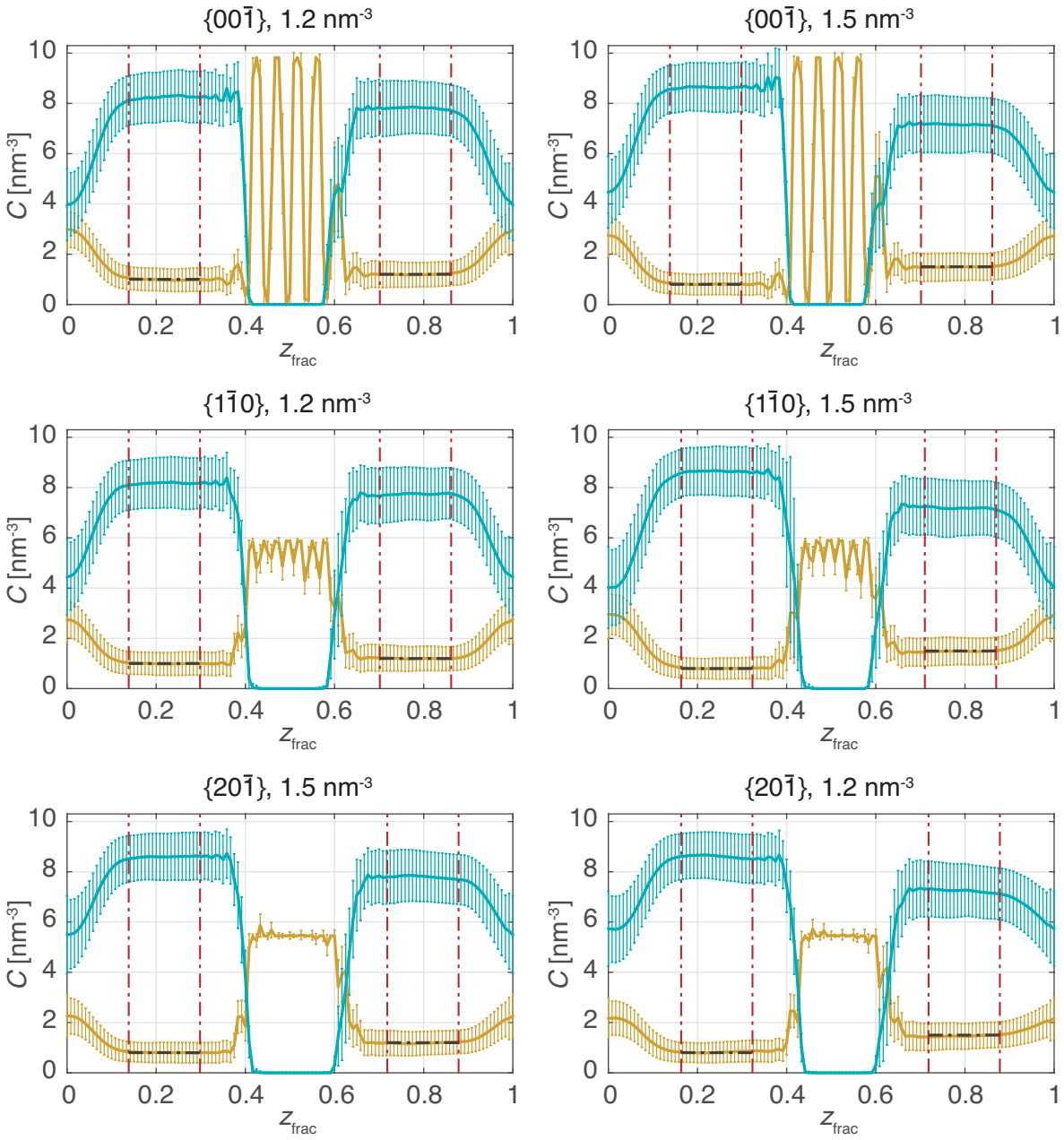

Figure 4: Concentration profiles along the z-axis (given as fractional coordinate) for the biased simulation averaged over 1 μs. The green lines correspond to the ethanol concentration and the khaki lines correspond to the naphthalene concentration. Error bars depict the standard deviation in the given segment. The red dashed lines indicate the boundaries of the control regions, in which the black dashed lines correspond to the target concentrations.

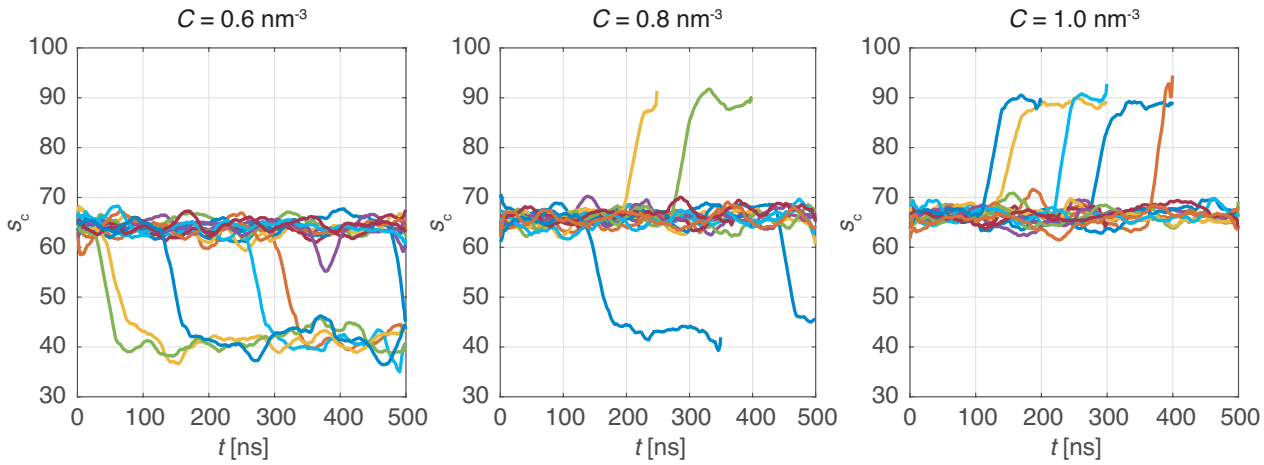

Figure 5: Unbiased CμMD simulation runs for three different naphthalene concentrations: system crystallinity, s_c, in dependence of time. The trajectories were smoothed out with a moving averge filter using a smoothing time of 3 ns to provide a clearer picuture of the growth and dissolution events.

Use of wall potentials for biased simulations

A lower and an upper wall potential were set to constrain the sampling to the relevant region:

$$V_\mathrm{w} = \begin{cases} w_\mathrm{l}(s - s_\mathrm{l})^2, & \text{if } s \leq s_\mathrm{l}, \\ 0, & \text{if } s_\mathrm{l} < s \leq s_\mathrm{u}, \\ w_\mathrm{u}(s - s_\mathrm{u})^2, & \text{else.} \end{cases} \tag{1}$$

The lower wall potential inhibits s from getting stuck at the value of zero, causing the biased simulation to crash. While the upper wall plays the important role of not letting the system completing the biased layer, since it would increase the convergence time significantly. As already indicated by Piana *et al.*,[15] the removal of solvent molecules from the remaining surface gap of the almost fully grown layer corresponds to a slow process. The upper wall potential prevents the system from reaching the CV space where the surface gap would emerge.

Table 6: Wall potential parameters used for s.

	$\{00\bar{1}\}$		$\{1\bar{1}0\}$		$\{20\bar{1}\}$	
C [nm^{-3}]	1.2	1.5	1.2	1.5	1.2	1.5
w_{l} [kJ/mol]	75	75	50	50	50	50
s_{l} [-]	0.07	0.07	0.07	0.07	0.07	0.07
w_{u} [kJ/mol]	10	10	25	25	10	25
s_{u} [-]	7.0	7.0	3.5	3.5	3.5	3.0

Surface layer crystallinity trajectories

The trajectories of the surface layer crystallinity CV, s_{slc}, of the biased simulations are shown in Figure 6. The first 200 ns of s_{slc} were not considered in the reweighting procedure[16] for all reweighted plots reported in the main text.

Numerical values for the interplanar spacing

Numerical values for the interplanar spacing, $d_{\{hkl\}}$, used for the calculation of the steady state crystal shape can be found in Table 7. The values were obtained from NPT simulations of a crystal of size $\sim 3 \times 3 \times 3$ nm^3 by using the anisotropic Parrinello-Rahman barostat[2] and taking the average lengths of $d_{\{hkl\}}$. The NPT simulations were performed for 10 ns each.

Table 7: Layer thickness, $d_{\{hkl\}}$, and simulation box surface area, $S_{\{hkl\}}$.

	$\{00\bar{1}\}$	$\{1\bar{1}0\}$	$\{20\bar{1}\}$
$d_{\{hkl\}}$ [nm]	0.929	0.451	0.410

References

(1) J. Wang, R. Wolf, J. Caldwell, P. Kollmann, D. Case, *J. Comput. Chem.* **25** (2004) 1157.

(2) M. Parrinello, A. Rahman, *J. Appl. Phys.* **52** (1981) 7182.

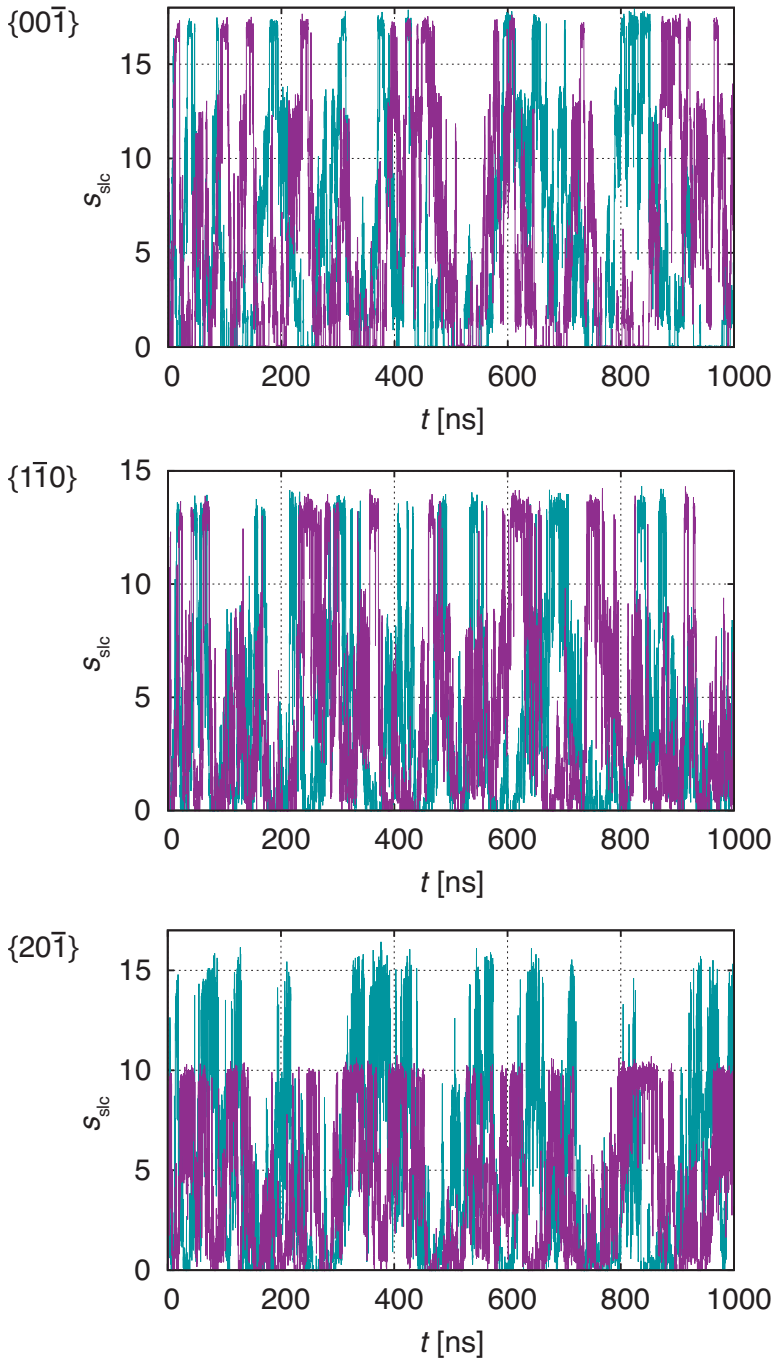

Figure 6: Trajectories of the surface layer crystallinity CV, s_{slc}, obtained from the biased simulations. Green denotes the concentration at $C = 1.2$ nm^{-3}, and purple denotes the concentration at $C = 1.5$ nm^{-3}.

(3) D. W. J. Cruickshank, *Acta Cryst.* **10** (1957) 504.

(4) G. Bussi, T. Zykova-Timan, M. Parrinello, *J. Chem. Phys.* **130** (2009) 074101.

(5) M. Salvalaglio, T. Vetter, F. Giberti, M. Mazzotti, M. Parrinello, *J. Am. Chem. Soc.* **134** (2012) 177221.

(6) D. H. Andrews, G. Lynn, J. Johnston *J. Am. Chem. Soc.* **48** (1926) 1274.

(7) M. J. Abraham, T. Murtola, R. Schulz, S. Pall, J. C. Smith, B. Hess, and E. Lindahl, *SoftwareX* **1** (2015) 19.

(8) T. Darden, D. York, and L. Pedersen, *J. Chem. Phys.* **98** (1993) 10089.

(9) B. Hess, *J. Chem. Theory Comput.* **4** (2008) 116

(10) B. Hess, C. Kutzner, E. Lindahl, *J. Chem. Theory Comput.* **4** (2008) 435.

(11) R. F. P. Grimbergen, M. F. Reedijk, H. Meekes, P. Bennema, *J. Phys. Chem. B* **102** (1998) 2646.

(12) M. A. Lovette and M. F. Doherty, *Cryst. Growth Des.* **12** (2012) 656.

(13) C. Perego, M. Salvalaglio, M. Parrinello, *J. Chem. Phys.* **142** (2015) 144113.

(14) G. A. Tribello, M. Bonomi, D. Branduardi, C. Camilloni, G. Bussi, *Comp. Phys. Comm.* **185** (2014) 604.

(15) S. Piana, J. D. Gale, *J. Am. Chem. Soc.* **127** (2005) 1975.

(16) P. Tiwary, M. Parrinello, *J. Phys. Chem. B* **119** (2015) 736.